Electronic Supplementary Information for

Excellent Intrinsic Chern insulators: Monolayer $PdTaX_2$ (X=Se, Te)

Shenda He,[1] Ruirong Kang,[1] Pan Zhou,[2,*] Pengbo Lyu,[1] and Lizhong Sun[1,†]

[1] *Hunan Provincial Key laboratory of Thin Film Materials and Devices, School of Materials Science and Engineering, Xiangtan University, Xiangtan 411105, China*
[2] *Key Laboratory of Low-dimensional Materials and Application Technology, School of Materials Science and Engineering, Xiangtan University, Xiangtan 411105, China*

(Dated: February 15, 2024)

* Electronic address: zhoupan71234@126.com
† Electronic address: lzsun@xtu.edu.cn

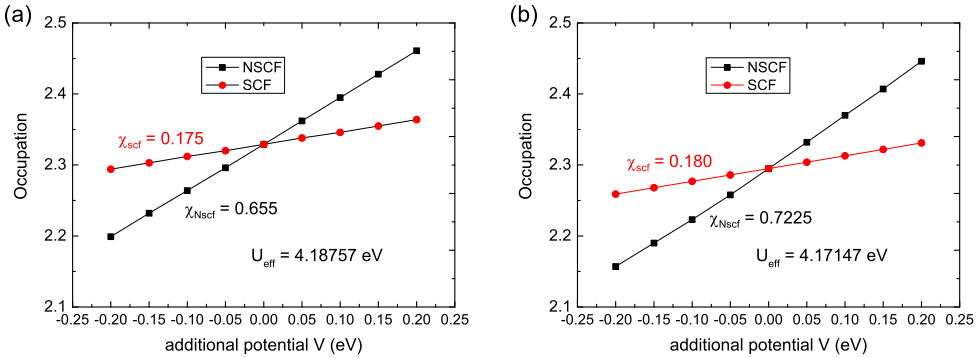

Figure S1: The U_{eff} for Ta in $PdTaSe_2$ and $PdTaTe_2$ monolayers.

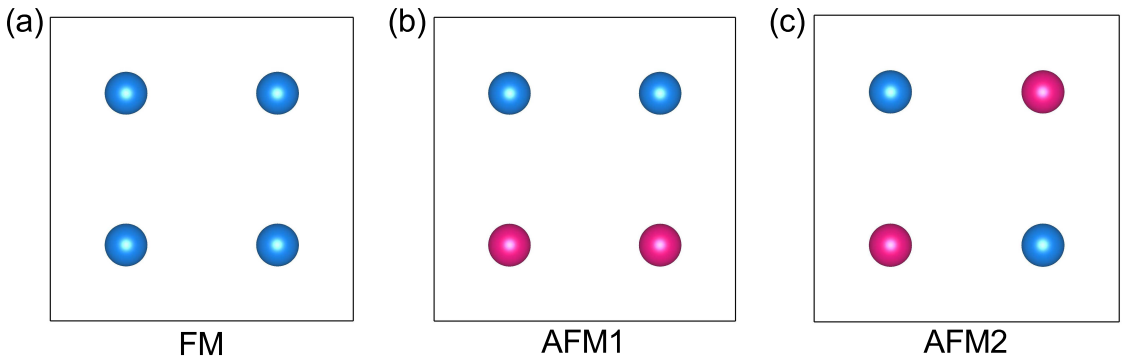

Figure S2: The different magnet configurations we employed to test the ground state, in which the $2 \times 2 \times 1$ supercell is used. The blue and purple represent the spin up or spin down Ta atoms, respectively.

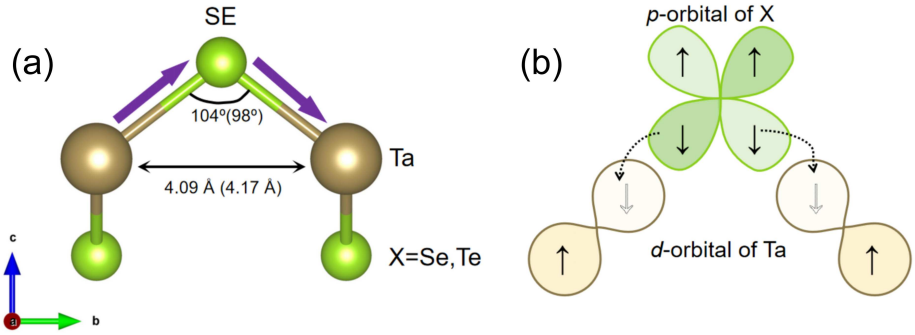

Figure S3: (a) The schematic diagram of the super-exchange (SE, Purple arrow), in which X atom represent Se or Te atoms. The angel and distance of Ta-Se-Ta(Ta-Te-Ta) is $104^o(98^o)$ and 4.09(4.17) Å. (b) Schematic diagram of the electrons hoping between X and Ta atoms.

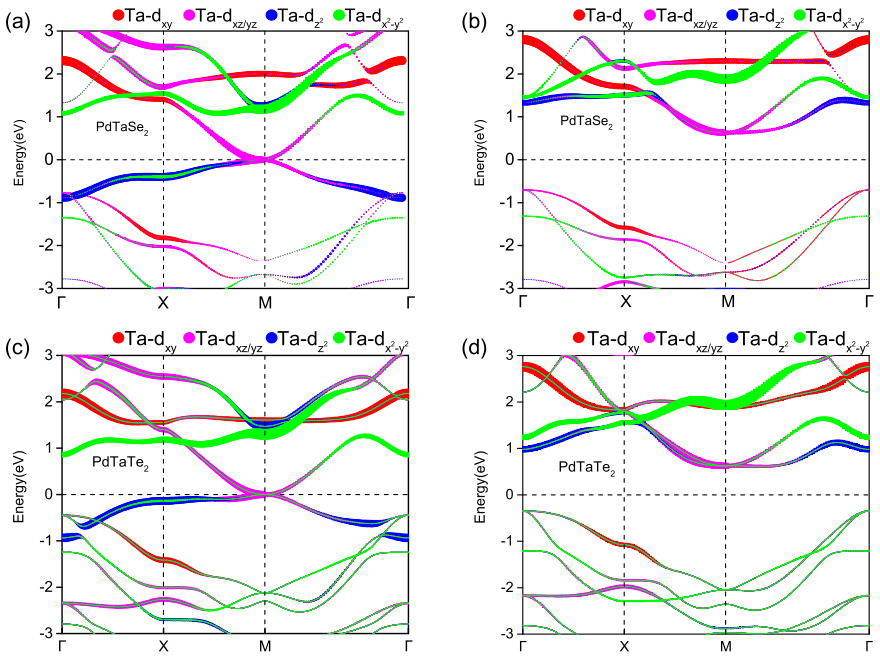

Figure S4: The orbital resolved band structures of $PdTaSe_2$ and $PdTaTe_2$ monolayers, respectively.(a) and (b) are the spin-up and spin-dn channel for the d orbitals of Ta for $PdTaSe_2$, while (c) and (d) depict the corresponding channels for $PdTaTe_2$.

Table S1: The Bader charge transfer of the two monolayers.

Elements	Pd	Ta	Se
$PdTaSe_2$	+0.479|e|	-1.681|e|	+0.601|e|
$PdTaTe_2$	+0.667|e|	-1.473|e|	+0.403|e|

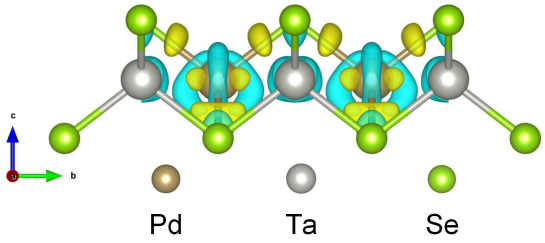

Figure S5: Differential charge density of $PdTaSe_2$, where yellow(blue) represents gained(lost) electrons.

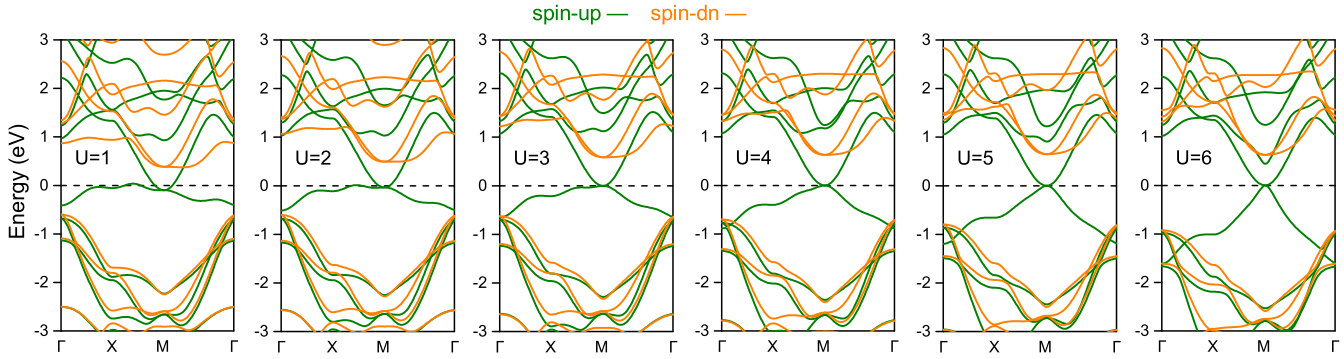

Figure S6: The band structures with the U_{eff} from 1 to 6 eV for $PdTaSe_2$. All of the E_f are set to zero.

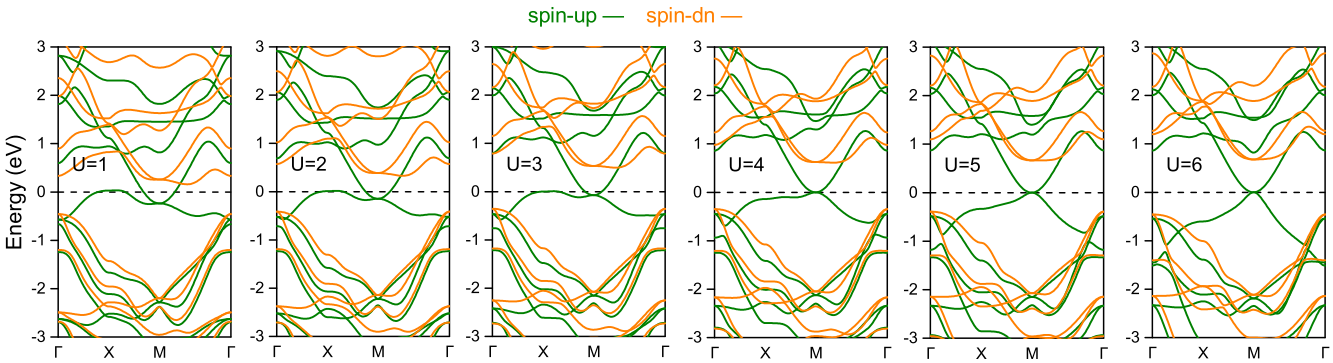

Figure S7: The band structures with the U_{eff} from 1 to 6 eV for $PdTaTe_2$. All of the E_f are set to zero.

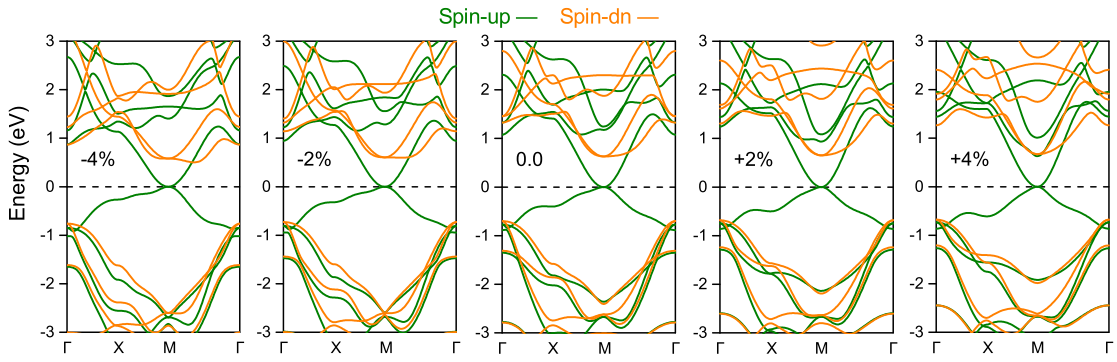

Figure S8: The band structures of $PdTaSe_2$ monolyer under biaxial strains ranging from -4% to $+4\%$. All of the E_f are set to zero.

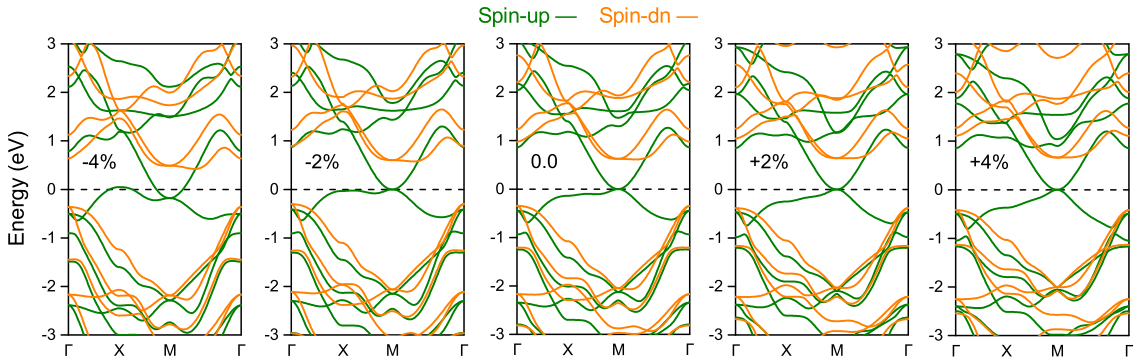

Figure S9: The figures present the band structures of $PdTaTe_2$ monolyer under biaxial strains ranging from -4% to $+4\%$. All of the E_f are set to zero.

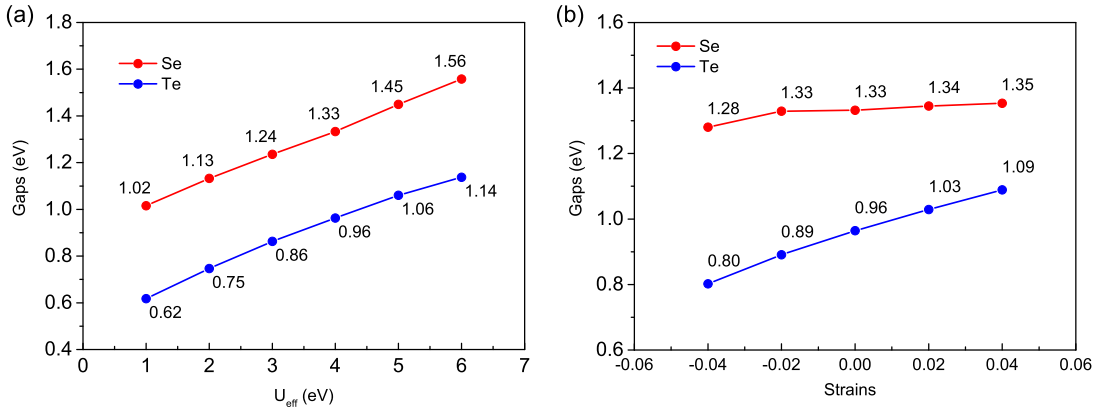

Figure S10: The spin gaps of the spin down channel for $PdTaSe_2$(in red) and $PdTaTe_2$(in blue) with different values of U_{eff} or a range of biaxial strains.

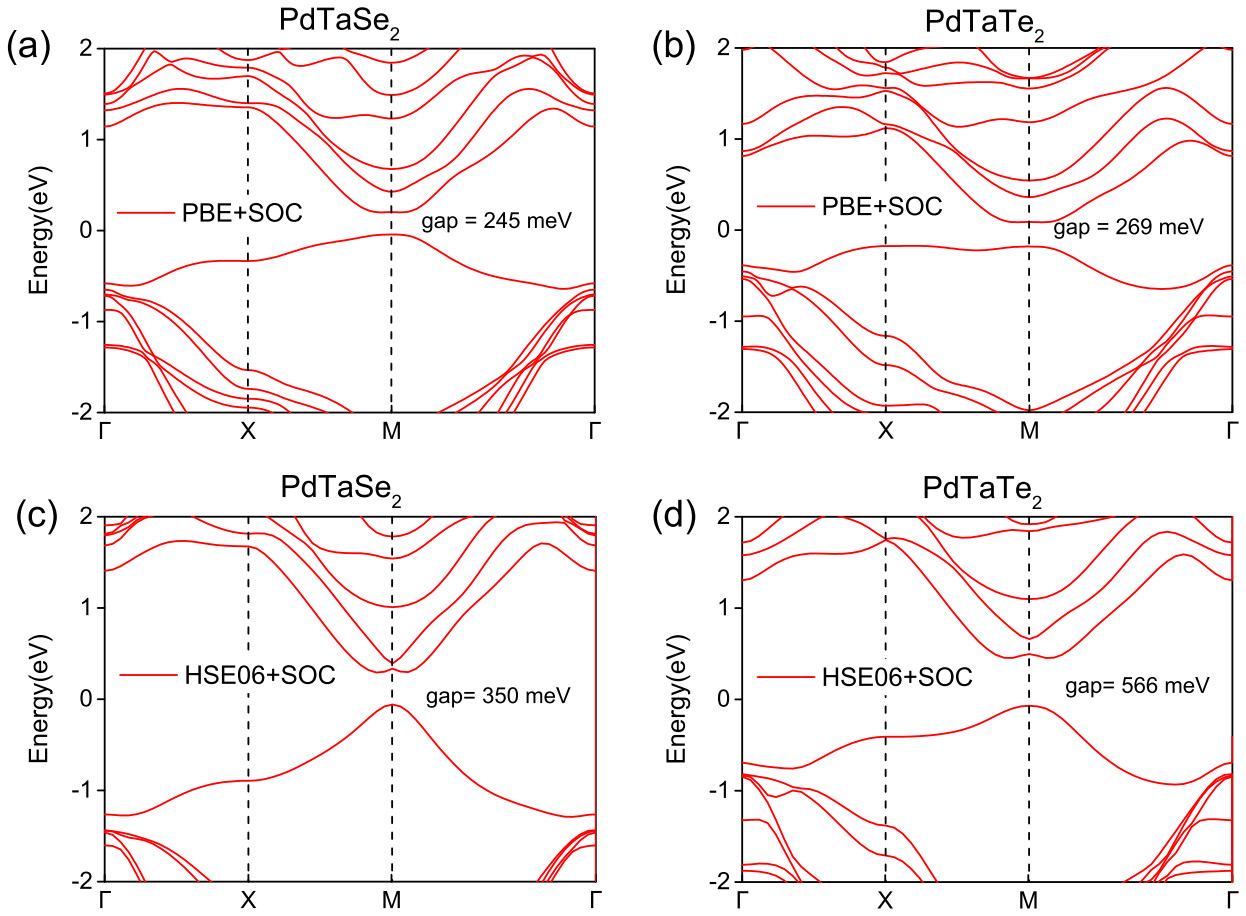

Figure S11: The orbital resolved band structures of $PdTaSe_2$ and $PdTaTe_2$ monolayers, respectively.(a) and (b) are the spin-up and spin-dn channel for the d orbitals of Ta for $PdTaSe_2$, while (c) and (d) depict the corresponding channels for $PdTaTe_2$.

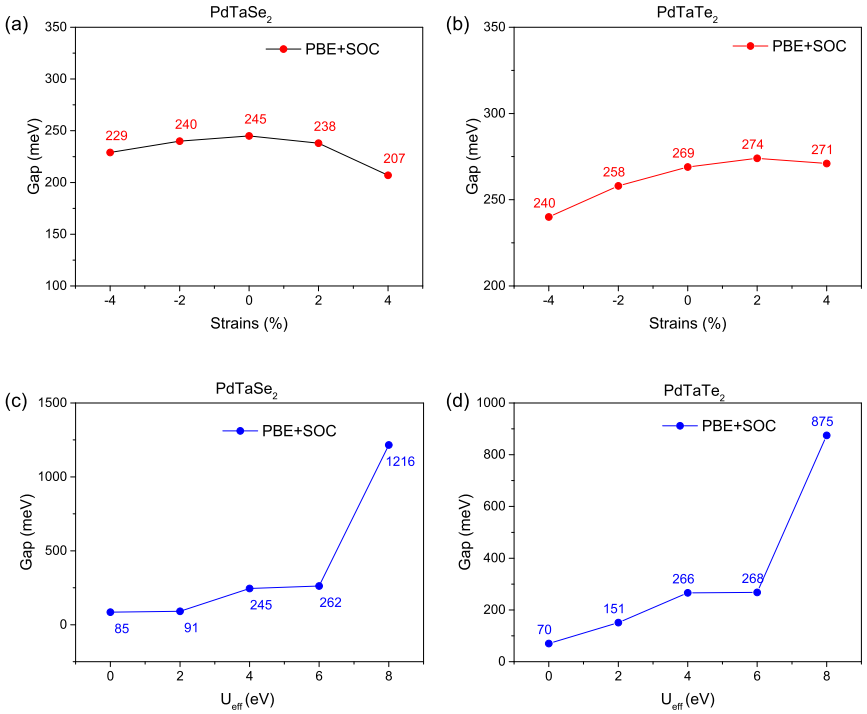

Figure S12: (a) and (b) depict the band gaps for $PdTaSe_2$ and $PdTaTe_2$ under strains ranging from -4% to 4% with spin-orbit coupling (SOC). In (c) and (d), the band gaps for these materials are presented under various U_{eff} values.

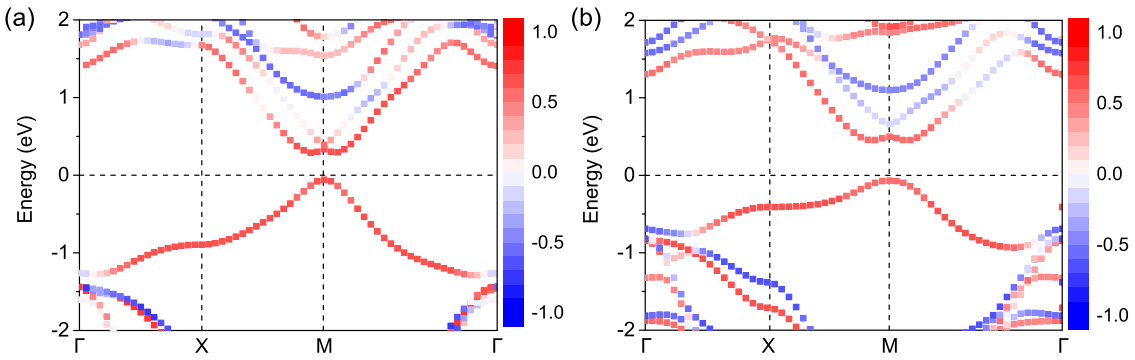

Figure S13: (a) and (b) are the normalized spin-resolved band structures of the $PdTaSe_2$ and $PdTaTe_2$ monolayers obtained by HSE06 functional in the presence of SOC, with the easy magnetization direction of the z axis.

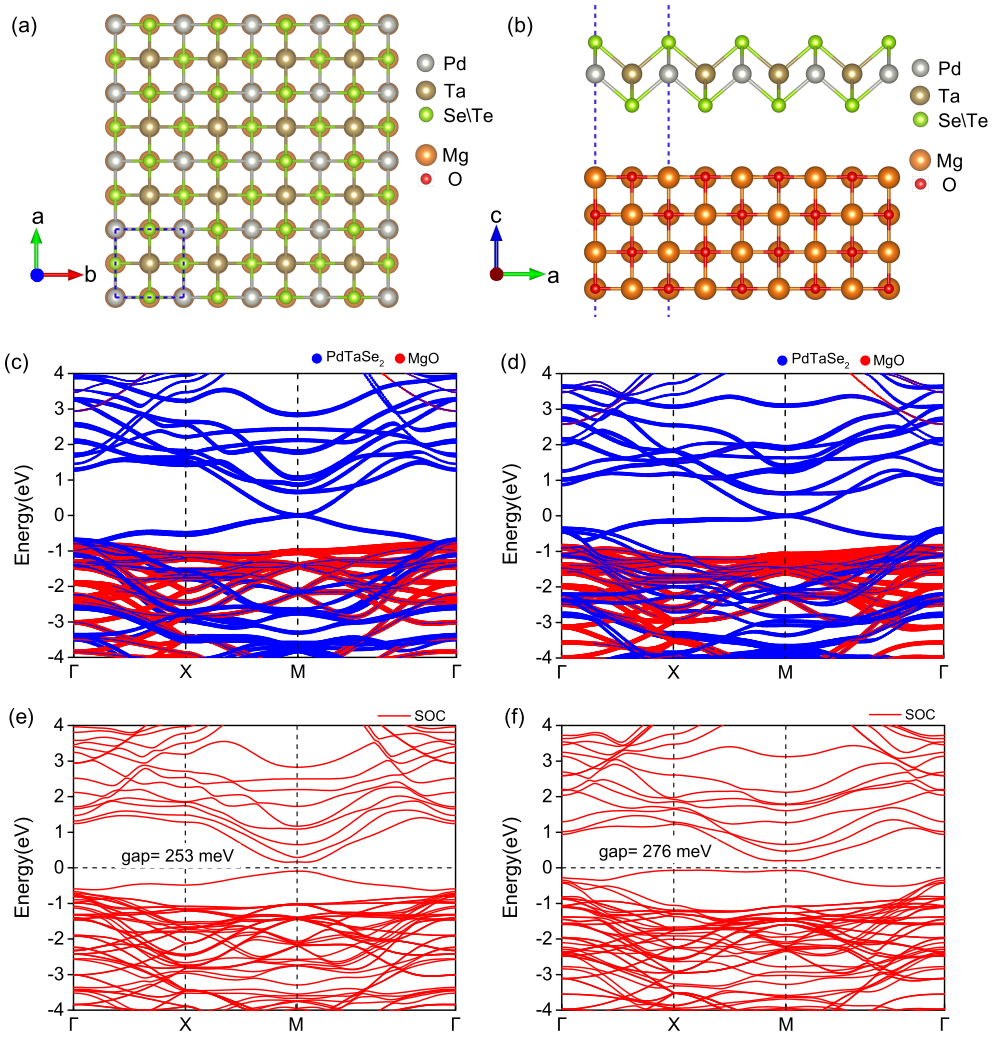

Figure S14: (a) and (b) are the top and side views of the equilibrium adsorption structure for the two monolayer adsorbed on a reconstructed MgO-(001) surface. The interlayer spaces for $PdTaSe_2$/MgO and $PdTaTe_2$/MgO are measured to be 3.63 Å and 4.08 Å, respectively. Band structures without spin-orbit coupling (SOC) are shown in (c) and (d) for $PdTaSe_2$/MgO and $PdTaTe_2$/MgO, while (e) and (f) display the band structures with SOC is considered.

Table S2: The comparison of some previously proposed 2D FM materials with ours.T_c is Curie temperature. TG or T denotes whether the gap type is topological and global or topological but not global. The calculation or fabrication methods are also listed for each materials.(ME: Mechanical exfoliation, MBE: molecular beam epitaxy, SF: self-flux method)

Materials	T_c	gap	TG or T	QAHE	methods	ref.
CrI_3	45	/	/	N	ME	Comput. Mater. Sci. 197, 110638 (2021)
$CrGeTe_3$	30	/	/	N	ME	Nature 546, 265 (2017)
Fe_5GeTe_2	280	/	/	N	ME	ACS nano 13, 4436 (2019).
VSe_2/MoS_2	300	/	/	N	MBE	Nanotechnol. 13, 289 (2018).
Cr_3Te_4	344	/	/	N	MBE	Adv. Mater. 33, 2103360 (2021)
Fe_3GaTe_2	380	/	/	N	SF	Nat. Commun. 13, 5067 (2022)
GaFeSe	1280	/	/	N	DFT	Phys. Rev. B 106, 125404 (2022)
InFeSe	1028	403	TG	Y	DFT	Phys. Rev. B 106, 125404 (2022)
TlFeSe	980	/	/	N	DFT	Phys. Rev. B 106, 125404 (2022)
$MnBi_2Se_4/Bi_2Se_3$	>300	100	TG	Y	MBE	Nano Lett. 17, 3493 (2017).
$(Bi_{0.8}Mn_{0.2})_2Se_3$	12	16	TG	Y	DFT	Phys. Rev. lett. 109, 076801 (2012).
$Co_3Pb_3Se_2$	42	77	TG	Y	DFT	Phys. Rev. B 103, 014410 (2021).
$Pb_3Pt_2Cl_9$	248	100	TG	Y	DFT	Phys. Rev. B 104, 205401 (2021)
TiTe	650	309	TG	Y	DFT	Nano Lett. 22, 5379 (2022).
LiFeSe	1500	35	TG	Y	DFT	Phys. Rev. lett. 125, 086401 (2020)
Fe_2IBr	403	260	TG	Y	DFT	Nanoscale 13, 12956 (2021)
Fe_2ICl	429	223	TG	Y	DFT	Nanoscale 13, 12956 (2021)
FeBr	417	166	TG	Y	DFT	J. Mater. Chem. C 10, 8381 (2022).
FeS	/	628	T	Y	DFT	Nat. Commun. 13, 919 (2022).
FeSe	/	798	T	Y	DFT	Nat. Commun. 13, 919 (2022).
$PdTaSe_2$	1049	334	TG	Y	DFT	/
$PdTaTe_2$	1003	692	TG	Y	DFT	/